Parametric Analysis of the Vibration Control of Sandwich Beams Through Shear-Based Piezoelectric Actuation

M. A. TRINDADE,* A. BENJEDDOU AND R. OHAYON
Structural Mechanics and Coupled Systems Laboratory, Conservatoire National des Arts et Métiers, 2, rue Conté, 75003, Paris, France

ABSTRACT: This paper presents a comparative numerical analysis of shear and extension actuation mechanisms for the bending vibrations control of sandwich beams. The extension actuation mechanism denotes the use of through-thickness poled piezoelectric actuators bonded on the surfaces of the structure such that, when submitted to a through-thickness applied electric potential, these actuators produce axial stresses or strains. The shear actuation mechanism, in the contrary, is obtained through an embedded longitudinally poled piezoelectric actuator that, subjected to the same electric potential, produces shear stresses or strains. Theoretical and finite element models of a sandwich beam, capable of dealing with both mechanisms, are presented. The models are based on Bernoulli-Euler assumptions for the surface layers and Timoshenko ones for the core. An optimal state feedback control law is used to maximize the damping of the first four natural modes of the sandwich beam. The influence of important parameters variation, such as actuator thickness and structure/actuator modulus ratio, on the performance of the control system is analyzed under limited input voltage and induced beam tip transverse deflection. Results suggest that shear actuators can be more effective than extension ones for the control of bending vibrations.

INTRODUCTION

PIEZOELECTRIC materials are widely used for structural vibration control. Commonly, they are bonded on the surface of the structure and, when activated by an applied electric field, their induced membrane deformation controls the vibrations of the structure. In this case, constant through-thickness electric fields are imposed to a transversely poled piezoelectric actuator, using the so-called e_{31} piezoelectric constant. This defines the extension actuation mechanism which has been widely used on either active control applications (Chandra and Chopra, 1993; Crawley and Anderson, 1990) or hybrid active-passive damping treatments (Baz, 1997; Huang, Inman and Austin, 1996; Tomlinson, 1996; Varadan, Lim and Varadan, 1996).

Recently, developments in composites design have brought attention to the use of embedded actuators. Although extension actuators can be embedded to produce torsional deformation (Bent, Hagood and Rodgers, 1995) using Piezoelectric Fiber Composites with or without Interdigitated Electrodes (Hagood et al. 1993), for the control of bending vibrations, they are not optimal on embedded configurations. Some recent works presented shear actuators, that are longitudinally poled and, when subjected to transverse electric field, present shear deformations through the so-called e_{15} piezoelectric constant. This leads to the less known shear actuation mechanism. In fact, the shear mode may also be obtained by applying axial electric fields on standard transversely poled piezoelectric actuators. However, putting conductors on side surfaces is a difficult task and leads to small axial electric fields for plate-type actuators. So that one should prefer to apply transverse electric fields on axially poled actuators. Figure 1 illustrates both actuation mechanisms. Hence, a comparative numerical static analysis using a commercial finite element code has been performed by Sun and Zhang (1995), who proposed also a theoretical model for shear-based actuators (Zhang and Sun, 1996). It was shown that embedded shear actuators are subjected to lower stresses than surface-mounted extension actuators, under actuation.

Shear actuation mechanisms were also studied by the present authors. A sandwich beam finite element, using the mean and relative axial displacements of the core skins as main parameters, was developed and validated (Benjeddou, Trindade and Ohayon, 1997). A comparison of extension and shear actuation mechanisms in static and free-vibration analysis was then carried out using this element discretization (Benjeddou, Trindade and Ohayon, 2000). It showed that for bending, shear actuators induce distributed actuation moments in the structure [Figure 1(b)] unlike extension actuators which induce boundary point forces [Figure 1(a)]. Therefore, it is proposed that the shear actuation mechanism may lead to less problems of debonding in actuators boundaries and to minor dependence of the control performance on actuators position and length. To provide a better understanding of the energy dissipation characteristics of both mechanisms, another sandwich beam finite element was developed, using the surface layers mean and relative axial displacements as independent variables (Benjeddou, Trindade and Ohayon, 1999b). Comparisons between the two finite elements showed that the second one presents better and faster

*Author to whom correspondence should be addressed.

1530-8138/99/05 0377-09 $10.00/0 DOI: 10.1106/UB60-GCGT-1PP6-2HKY

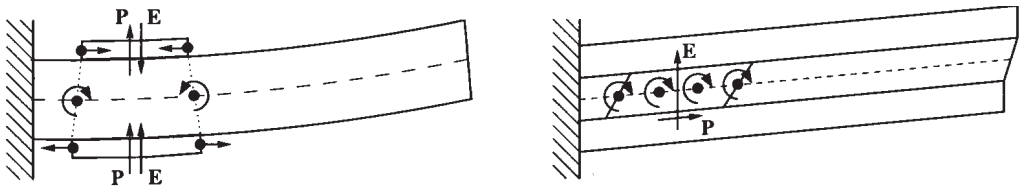

a) Extension actuation mechanism b) Shear actuation mechanism

Figure 1. *Piezoelectric extension and shear actuation mechanisms.*

convergence (Benjeddou, Trindade and Ohayon, 1999a). That is why it was retained for current and future researches.

Using the strain-induced piezoelectric coupling constant d_{15}, Kim et al. (1997) have recently proposed composite piezoelectric assemblies for shear-based torsional actuators for the production of large angular displacement and torque. They discussed actuator designs and assembly methods, material preparation, poling procedures, test results for joint strengths, and actuator output capabilities. It was pointed out that commercially available PZT piezoelectrics are optimized for their extension response but not for their shear behavior.

This paper aims to present a comparative study of shear and extension actuation mechanisms for structural bending vibration control. Theoretical and finite element models together with an LQR optimal control strategy are presented. Then, under limited input voltage and induced beam tip transverse deflection, these are used to study control performances of both mechanisms through parameters variations, such as actuator thickness, structure/actuator modulus ratio and core filling material properties.

THEORETICAL FORMULATION

Two configurations of a symmetric three-layer sandwich beam are considered. In the first one, an elastic central core is sandwiched between two transversely poled piezoelectric layers [Figure 1(a)], whereas, in the second one, two elastic layers sandwich a longitudinally poled piezoelectric core [Figure 1(b)]. For both cases, a transverse electric field is applied to piezoelectric layers, which have electrodes on top and bottom skins. However, elastic layers are assumed insulated. All layers are assumed perfectly bonded and in plane stress state. Top and bottom layers are assumed to behave as Bernoulli-Euler beams, whereas Timoshenko theory is retained for the central core to allow shear deformation. This is necessary for the shear actuation mechanism. Local axes are attached to surface layers at their left end centers, and a global one is attached to the left end center of the beam, so that beam centroidal and elastic axes coincide with the x-axis. The length, width and thickness of the beam are denoted by L, b and h, respectively. a, b, c indices indicate top, bottom and core layers quantities and f index is used for surface layer parameters. The geometrical and kinematics descriptions of the sandwich beam are given in Figure 2.

Mechanical Displacements and Strains

Starting with linear axial displacements for each layer and enforcing the interface displacement continuities, the following expressions for the surface layers and core axial displacements are obtained

$$\hat{u}_k = \left(\overline{u} \pm \frac{\tilde{u}}{2}\right) - (z - z_k)w';$$

$$k = a,b \ (+ \text{ for } k = a \text{ and } - \text{ for } k = b) \tag{1}$$

$$\hat{u}_c = \overline{u} + z\left(\frac{\tilde{u}}{h_c} + \lambda w'\right); \quad \lambda = \frac{h_f}{h_c}$$

Where $z_a = (h_a + h_c)/2$, $z_b = -(h_b + h_c)/2$ and w' is the first derivative of the transverse deflection w, supposed constant through-thickness. $\overline{u}$ and $\tilde{u}$ are the mean and relative axial displacements of the surface layers, defined by,

$$\overline{u} = \frac{u_a + u_b}{2}; \quad \tilde{u} = u_a - u_b \tag{2}$$

here, u_a and u_b are mid-plane displacements of the top and bottom layers (Figure 2).

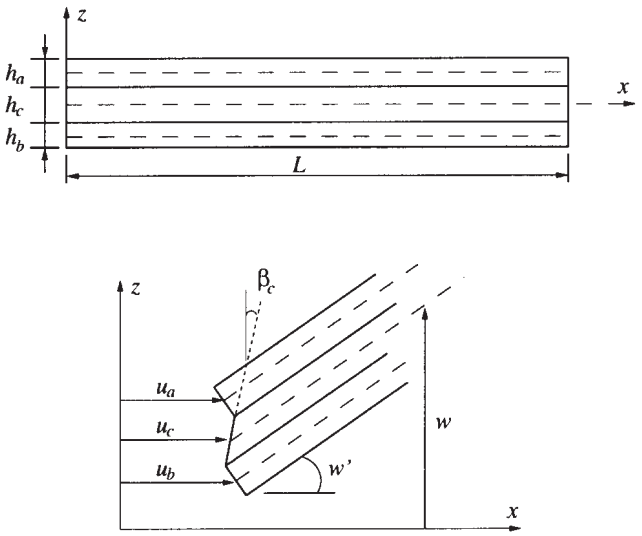

Figure 2. *Geometrical and kinematics descriptions of the sandwich beam.*

From the above displacements and usual strain-displacement relations, layers strains can be written as

$$\varepsilon_{k1} = \varepsilon_k^m + (z - z_k)\varepsilon_k^b; \quad \varepsilon_{c1} = \varepsilon_c^m + z\varepsilon_c^b;$$
$$\varepsilon_{c5} = \varepsilon_c^s = \left[\frac{\tilde{u}}{h_c} + (\lambda + 1)w'\right] \tag{3}$$

where

$$\varepsilon_k^m = \bar{u}' \pm \frac{\tilde{u}'}{2}; \quad \varepsilon_k^b = -w''; \quad k = a(+), b(-);$$
$$\varepsilon_c^m = \bar{u}'; \quad \varepsilon_c^b = \left(\frac{\tilde{u}'}{h_c} + \lambda w''\right) \tag{4}$$

The mechanical parameter λ couples the bending behavior of the surface layers to that of the core. It is an important variable for parameter studies.

Piezoelectric Plane-Stress Reduced Constitutive Equations and Electric Potentials

The piezoelectric layers are considered to be linear orthotropic piezoelectric materials with material symmetry axes parallel to the beam axes. c_{jl}, e_{ml} and ϵ_{mm} ($j,l = 1, \ldots, 6$; $m = 1, 2, 3$) denote their elastic, piezoelectric and dielectric constants.

For extension actuation mechanism, supposing a plane-stress state ($\sigma_3 = 0$), the three-dimensional linear constitutive equations of an orthotropic piezoelectric layer can be reduced to (for reduction details, see Benjeddou, Trindade and Ohayon, 1997)

$$\begin{Bmatrix}\sigma_1\\ D_3\end{Bmatrix} = \begin{bmatrix}c_{11}^* & -e_{31}^*\\ e_{31}^* & \epsilon_{33}^*\end{bmatrix}\begin{Bmatrix}\varepsilon_1\\ E_3\end{Bmatrix} \tag{5}$$

where

$$c_{11}^* = c_{11} - \frac{c_{13}^2}{c_{33}}; \quad e_{31}^* = e_{31} - \frac{c_{13}}{c_{33}}e_{33}; \quad \epsilon_{33}^* = \epsilon_{33} + \frac{e_{33}^2}{c_{33}}$$

σ_1, ε_1, D_3 and E_3 are axial stress and strain, and transverse electric displacement and field. Notations of the IEEE Standard on Piezoelectricity (1987) are retained here. Notice that the piezoelectric effect couples only axial strain and transverse electric field, characterizing an extension actuation mechanism.

For the shear actuation mechanism, it can be shown (for details see Benjeddou, Trindade and Ohayon, 1997) that, after coordinate transformations (Bent, Hagood and Rodgers, 1995; Hagood et al., 1993) so that axial and transverse indices interchange, the three-dimensional linear constitutive equations of the orthotropic piezoelectric core reduce to,

$$\begin{Bmatrix}\sigma_1\\ \sigma_5\\ D_3\end{Bmatrix} = \begin{bmatrix}c_{33}^* & 0 & 0\\ 0 & c_{55} & -e_{15}\\ 0 & e_{15} & \epsilon_{11}\end{bmatrix}\begin{Bmatrix}\varepsilon_1\\ \varepsilon_5\\ E_3\end{Bmatrix} \tag{6}$$

where

$$c_{33}^* = c_{33} - \frac{c_{13}^2}{c_{11}}$$

σ_5 and ε_5 are transverse shear stress and strain. Here, the piezoelectric effect couples shear strain and transverse electric field, characterizing a shear actuation mechanism.

The combination of the strain-displacement relations obtained from Equations (1)–(4), and the reduced constitutive Equations (5) or (6), then integration of the electrostatic equilibrium equation, free of volumic charge density, allow us to write the following electric potential forms for piezoelectric surface layers φ_k (extension actuation mechanism), and for a piezoelectric core φ_c (shear actuation mechanism), respectively

$$\varphi_k = \bar{\varphi}_k + (z - z_k)\frac{\tilde{\varphi}_k}{h_f} + \left[1 - \frac{4(z - z_k)^2}{h_f^2}\right]\frac{h_f^2}{8}\frac{e_{31}^{f*}}{\epsilon_{33}^{f*}}w'' \tag{7}$$

$$\varphi_c = \bar{\varphi}_c + z\frac{\tilde{\varphi}_c}{h_c} \tag{8}$$

where

$$\bar{\varphi}_i = \frac{\varphi_i^+ + \varphi_i^-}{2}; \quad \tilde{\varphi}_i = \varphi_i^+ - \varphi_i^-; \quad i = a,\ b,\ c$$

are the mean and the difference of the prescribed electric potentials on top (φ_i^+) and bottom (φ_i^-) skins of the i-th layer. The last term in Equation (7) represents the quadratic induced potential, often neglected in the literature (Rahmoune et al., 1998).

Variational Formulation

In order to study the effects of the electromechanical coupling on the dynamics of the sandwich beam, let us start from the following variational formulation of the problem in terms of the unknown fields $\bar{u}$, $\tilde{u}$, w and $\tilde{\varphi}$

$$\delta T - \delta H + \delta W = 0; \quad \forall \delta\bar{u},\ \delta\tilde{u},\ \delta w,\ \delta\tilde{\varphi} \tag{9}$$

where δT, δH and δW are the virtual variations of kinetic energy $T(\bar{u},\tilde{u},w)$, electromechanical energy $H(\bar{u},\tilde{u},w,\varphi)$ and work done by applied mechanical loads $W(\bar{u},\tilde{u},w)$, respectively. Here only the actuation problem is considered, that is, $\tilde{\varphi}_i$ are given. Thus, only $\bar{u}$, $\tilde{u}$ and w must be retained as independent and unknown fields. Note that these fields are time and space-dependent, whereas their variations

$(\delta\bar{u},\delta\tilde{u},\delta w)$ are only space-dependent. Therefore, the virtual variations in Equation (9) are now detailed in terms of these three main variables, only. It is important to notice that the Equation (9) must be complemented by initial conditions.

To provide a better understanding of the extension and shear actuation mechanisms, surface layers and core contributions (δH_f and δH_c) to the electromechanical energy variation are studied separately

$$\delta H = \delta H_f + \delta H_c \tag{10}$$

Decomposing these two variations into mechanical and electromechanical contributions, the surface layers contribution δH_f is written as

$$\delta H_f = \delta \bar{H}_{fm} - \delta H_{fme} \tag{11}$$

where,

$$\delta \bar{H}_{fm} = 2\int_0^L \left\{ c_{11}^{f*} A_f \bar{u}'\delta\bar{u}' + \frac{1}{4} c_{11}^{f*} A_f \tilde{u}'\delta\tilde{u}' + \bar{c}_{11}^{f} I_f w''\delta w'' \right\} dx$$

$$\delta H_{fme} = -\int_0^L e_{31}^{f*} \frac{A_f}{h_f} \left[(\tilde{\varphi}_a + \tilde{\varphi}_b)\delta\bar{u}' + (\tilde{\varphi}_a - \tilde{\varphi}_b)\frac{\delta\tilde{u}'}{2} \right] dx$$

and the core contribution δH_c as

$$\delta H_c = \delta H_{cm} - \delta H_{cme} \tag{12}$$

where,

$$\delta H_{cm} = \int_0^L \left\{ \begin{array}{l} c_{33}^{c*} A_c \bar{u}'\delta\bar{u}' + c_{33}^{c*} I_c \left(\dfrac{\tilde{u}'}{h_c} + \lambda w'' \right)\left(\dfrac{\delta\tilde{u}'}{h_c} + \lambda\delta w'' \right) \\ + \mathrm{c}_{55}^{\mathrm{c}} A_c \left[\dfrac{\tilde{u}}{h_c} + (\lambda+1)w' \right]\left[\dfrac{\delta\tilde{u}}{h_c} + (\lambda+1)\delta w' \right] \end{array} \right\} dx$$

$$\delta H_{cme} = -\int_0^L e_{15}^{c} A_c \frac{\tilde{\varphi}_c}{h_c} \left[\frac{\delta\tilde{u}}{h_c} + (\lambda+1)\delta w' \right] dx$$

In Equations (11) and (12), I_i, A_i are moment area and area of the i-th layer. Notice that the induced potential leads to an augmentation of the surface layers bending stiffness through

$$\bar{c}_{11}^{f} = c_{11}^{f*} + \frac{(e_{31}^{f*})^2}{\epsilon_{33}^{f*}}$$

From Equation (12), δH_{cme} can be interpreted as a distributed moment $e_{15}^{c} A_c \tilde{\varphi}_c / h_c$ induced by the applied electric difference of potential $\tilde{\varphi}_c$ to the core layer [Figure 1(b)]. A transverse shear strain $[\tilde{u}/h_c + (\lambda+1)w']$ is then produced.

Since, only the bending actuation will be considered here, surface imposed potentials are of opposite signs $(\tilde{\varphi}_a = -\tilde{\varphi}_b = \tilde{\varphi}_f)$. Hence, δH_{fme}, given in Equation (11), reduces to,

$$\delta \tilde{H}_{fme} = -\int_0^L e_{31}^{f*} A_f \frac{\tilde{\varphi}_f}{h_f} \delta\tilde{u}'dx = -e_{31}^{f*} A_f \frac{\tilde{\varphi}_f}{h_f} \delta\tilde{u} \Big|_0^L \tag{13}$$

Therefore, $\delta \tilde{H}_{fme}$ is interpreted as the virtual work of boundary point actuation tractions $e_{31}^{f*} A_f \tilde{\varphi}_f / h_f$ induced by the applied opposite difference of potentials $\tilde{\varphi}_f$ on the surface layers [Figure 1(a)]. Only relative axial displacement or strain of the surface layers is produced.

Comparing δH_{cme} in Equation (12) to $\delta \tilde{H}_{fme}$ in Equation (13), one can notice that the extension actuation mechanism produces boundary point forces (tractions/compressions), whereas the shear actuation mechanism induces distributed moments (Figure 1). Hence, one can expect that the latter avoids the common singularity problems at the boundaries of conventional extension actuators.

Variations of the kinetic energy and work due to applied mechanical loads of the sandwich beam for both mechanisms, written in terms of the main variables, are

$$\delta T = \int_0^L \left\{ \begin{array}{l} (2\rho_f A_f + \rho_c A_c)\ddot{\bar{u}}\delta\bar{u} \\ + \left[\left(2\rho_f A_f + 4\rho_c \dfrac{I_c}{h_c^2} \right)\dfrac{\ddot{\tilde{u}}}{2} + \rho_c \dfrac{I_c}{h_c}\lambda\ddot{w}' \right]\dfrac{\delta\tilde{u}}{2} \\ + (2\rho_f A_f + \rho_c A_c)\ddot{w}\delta w \\ + \left[\rho_c I_c \lambda \dfrac{\ddot{\tilde{u}}}{h_c} + (2\rho_f I_f + \rho_c I_c \lambda^2)\ddot{w}' \right]\delta w' \end{array} \right\} dx \tag{14}$$

and

$$\delta W = \int_0^L \left[\begin{array}{l} (n_a + n_b + n_c)\delta\bar{u} + \left(\dfrac{n_a - n_b}{2} + \dfrac{m_c}{h_c} \right)\delta\tilde{u} \\ - (m_a + m_b - \lambda m_c)\delta w' + (q_a + q_b + q_c)\delta w \end{array} \right] dx$$
$$+ \left[\begin{array}{l} (N_a + N_b + N_c)\delta\bar{u} + \left(\dfrac{N_a - N_b}{2} + \dfrac{M_c}{h_c} \right)\delta\tilde{u} \\ - (M_a + M_b - \lambda M_c)\delta w' + (Q_a + Q_b + Q_c)\delta w \end{array} \right]_0^L \tag{15}$$

where ρ_i is the mass density of the i-th layer. n_i, m_i, q_i and N_i, M_i, Q_i are distributed and point normal, moment and shear stress resultants.

For the extension actuation mechanism, δH_{cme} vanishes since the core is not piezoelectric. Thus, the variational Equation (9) reduces to

$$\delta \bar{H}_{fm} + \delta H_{cm} - \delta T = \delta W + \delta H_{fme}; \quad \forall \delta\bar{u}, \delta\tilde{u}, \delta w \tag{16}$$

Similarly, for the shear actuation mechanism, δH_{fme} vanishes since the surface layers are elastic. The variational Equation (9) is then

$$\delta H_{fm} + \delta H_{cm} - \delta T = \delta W + \delta H_{cme}; \quad \forall \delta\bar{u}, \delta\tilde{u}, \delta w \tag{17}$$

where δH_{fm} is similar to $\delta \bar{H}_{fm}$ but with $\bar{c}_{11}^{f} = c_{11}^{f*}$.

FINITE ELEMENT DISCRETIZATION

The standard finite element method is followed to discretize the variational problems Equations (16) and (17). The variables $\bar{u}$ and $\tilde{u}$ are interpolated by Lagrange linear shape functions and w by Hermite cubic ones. For the shear actuation mechanism, the discretized equations of motion can be written as,

$$\mathbf{M}\ddot{\mathbf{q}} + \mathbf{C}_v\dot{\mathbf{q}} + (\mathbf{K}_f + \mathbf{K}_c)\mathbf{q} = \mathbf{F}_m + \mathbf{F}_{ce}\tilde{\varphi}_c \tag{18}$$

where $\mathbf{q} = [\bar{u}_1, \tilde{u}_1, w_1, w_1', \bar{u}_2, \tilde{u}_2, w_2, w_2']$ is the vector of degrees of freedom and $\dot{\mathbf{q}}, \ddot{\mathbf{q}}$ the corresponding velocity and acceleration. $\mathbf{M}$ is the mass matrix obtained from the discretization of δT. $\mathbf{C}_v$ is a global viscous damping matrix accounting for materials damping. $\mathbf{K}_f$ and $\mathbf{K}_c$ are the surface layers and core stiffness matrices obtained from the discretization of $\delta \bar{H}_{fm}$ (with $\bar{c}_{11}^{f} = c_{11}^{f*}$) and δH_{cm} given in Equations (11) and (12), respectively. $\mathbf{F}_{ce}\tilde{\varphi}_c$ and $\mathbf{F}_m$ are the induced electric and mechanical load vectors deduced from discretization of δH_{cme} in Equation (12) and δW, respectively.

For the extension actuation mechanism, the discretization of Equation (17) leads to the following discretized equations of motion

$$\mathbf{M}\ddot{\mathbf{q}} + \mathbf{C}_v\dot{\mathbf{q}} + (\bar{\mathbf{K}}_f + \mathbf{K}_c)\mathbf{q} = \mathbf{F}_m + \mathbf{F}_{ce}\tilde{\varphi}_f \tag{19}$$

where $\bar{\mathbf{K}}_f$ is the stiffness matrix of the piezoelectric surface layers and $\mathbf{F}_{fe}\tilde{\varphi}_f$ is the induced electric force vector obtained from the discretization of Equation (13). All matrices and vectors of Equations (18) and (19) were integrated analytically and implemented in MATLAB software. A comprehensive review synthesis on the piezoelectric finite element literature was given by Benjeddou (2000).

CONTROL STRATEGY

Prior to the presentation of the vibration control strategy, linear second order matricial Equations (18) and (19), are written in state-space form, with state vector $\mathbf{x}$, input vector $\mathbf{u}$ and output vector $\mathbf{y}$,

$$\begin{cases} \dot{\mathbf{x}} = \mathbf{A}_j\mathbf{x} + \mathbf{B}_j\mathbf{u} + \mathbf{B}_p; \quad j = f, c \\ \mathbf{y} = \mathbf{C}\mathbf{x} \end{cases}; \quad \mathbf{x} = \begin{Bmatrix} \mathbf{q} \\ \dot{\mathbf{q}} \end{Bmatrix} \tag{20}$$

$\mathbf{A}_j$ and $\mathbf{B}_j$ ($j = f,c$) represent system and control matrices of the extension (f) and shear (c) actuation mechanisms, respectively. $\mathbf{B}_p$ represents the perturbations vector and $\mathbf{C}$, the state output matrix. These have the following expressions,

$$\mathbf{A}_f = \begin{bmatrix} \mathbf{0} & \mathbf{I} \\ -\mathbf{M}^{-1}(\bar{\mathbf{K}}_f + \mathbf{K}_c) & \mathbf{0} \end{bmatrix}; \quad \mathbf{A}_c = \begin{bmatrix} \mathbf{0} & \mathbf{I} \\ -\mathbf{M}^{-1}(\mathbf{K}_f + \mathbf{K}_c) & \mathbf{0} \end{bmatrix} \tag{21}$$

$$\mathbf{B}_f = \begin{bmatrix} \mathbf{0} \\ \mathbf{M}^{-1}\mathbf{F}_{fe} \end{bmatrix}; \quad \mathbf{B}_c = \begin{bmatrix} \mathbf{0} \\ \mathbf{M}^{-1}\mathbf{F}_{ce} \end{bmatrix}; \quad \mathbf{B}_p = \begin{bmatrix} \mathbf{0} \\ \mathbf{M}^{-1}\mathbf{F}_m \end{bmatrix} \tag{22}$$

For both configurations (surface-mounted or sandwich), it is supposed that the control actuation is done by the piezoelectric actuators only. Therefore, $\mathbf{B}_j$ and $\mathbf{B}_p$ are column vectors and $\mathbf{u}$ is a scalar, representing the imposed voltage $\mathbf{u} = \bar{\varphi}_f$ for the extension actuation mechanism and $\mathbf{u} = \tilde{\varphi}_c$ for the shear one.

The design of the controller is based on LQR full state feedback, i.e., the control voltage $\mathbf{u}$ is proportional to the state vector $\mathbf{x}$,

$$\mathbf{u} = -\mathbf{K}_g\mathbf{x} \tag{23}$$

where $\mathbf{K}_g$ is a row vector representing the control gain. Substituting Equation (23) in the uncontrolled state Equations (20), the resulting controlled ones can be written as

$$\begin{aligned} \dot{\mathbf{x}} &= (\mathbf{A}_j - \mathbf{B}_j\mathbf{K}_g)\mathbf{x} + \mathbf{B}_p \\ \mathbf{y} &= \mathbf{C}\mathbf{x} \end{aligned} \tag{24}$$

The system is then controlled by a modification of the matrix $\mathbf{A}_j$, which becomes $\mathbf{A}_j - \mathbf{B}_j\mathbf{K}_g$. Therefore, the control action may stabilize the system by changing its vibration characteristics, such as the damping of some chosen poles, as explained in the following section.

In order to interpret these results in a structural mechanics approach, Equations (18) and (19) can be rewritten, taking into account Equations (21), (22) and (24), as

$$\mathbf{M}\ddot{\mathbf{q}} + (\mathbf{C}_v + \mathbf{F}_{ce}\mathbf{K}_d)\dot{\mathbf{q}} + (\mathbf{K}_f + \mathbf{K}_c + \mathbf{F}_{ce}\mathbf{K}_p)\mathbf{q} = \mathbf{F}_m \tag{25}$$

for the shear actuation mechanism, and

$$\mathbf{M}\ddot{\mathbf{q}} + (\mathbf{C}_v + \mathbf{F}_{fe}\mathbf{K}_d)\dot{\mathbf{q}} + (\bar{\mathbf{K}}_f + \mathbf{K}_c + \mathbf{F}_{fe}\mathbf{K}_p)\mathbf{q} = \mathbf{F}_m \tag{26}$$

for the extension one. The row vectors $\mathbf{K}_d$ and $\mathbf{K}_p$ are obtained from decomposition of the gain row vector into proportional and derivative components, i.e., $\mathbf{K}_g = [\mathbf{K}_p \ \mathbf{K}_d]$. One can notice that the control law supplies a stiffness matrix $\hat{\mathbf{K}} = \mathbf{F}_{je}\mathbf{K}_p$ and a damping matrix $\hat{\mathbf{C}} = \mathbf{F}_{je}\mathbf{K}_d$ in addition to the actual structural stiffness matrices and eventual initial viscous damping matrix $\mathbf{C}_v$. The unified resulting system may be represented by the general form

$$\mathbf{M}\ddot{\mathbf{q}} + (\mathbf{C}_v + \hat{\mathbf{C}})\dot{\mathbf{q}} + (\mathbf{K} + \hat{\mathbf{K}})\mathbf{q} = \mathbf{F}_m \tag{27}$$

where $\mathbf{K} = \bar{\mathbf{K}}_f + \mathbf{K}_c$ for the extension actuation mechanism and $\mathbf{K} = \mathbf{K}_f + \mathbf{K}_c$ for the shear one. It is worthwhile to compare the original uncontrolled systems (18) and (19) with the corresponding controlled systems (25) and (26). The LQR control strategy is implemented using MATLAB Control Toolbox.

NUMERICAL RESULTS

This section aims to present a comparative numerical analysis of shear and extension actuation mechanisms. To this end, the present finite element model is used to evaluate bending vibration characteristics of both mechanisms (Figure 3), under variations of several parameters such as, actuator thickness, structure/actuator modulus ratio, foam stiffness and number of actuators.

The geometrical data of the beam, according to Figure 3, are $L = 200$ mm, $h = 4$ mm, $t = 0.05$ mm, $d_c = 30$ mm, $a = 30$ mm. The shear actuator thickness is $2t$ leading to equivalent surface-mounted and sandwich configurations. Aluminum properties are: Young's modulus $E_b = 70.3$ GPa, Poisson's ratio $\nu = 0.35$, density $\rho_b = 2710$ kg m^{-3}. Those of the foam are: Young's modulus $E_f = 35.3$ MPa, shear modulus $G_f = 12.7$ MPa, density $\rho_f = 32$ kg m^{-3}; and, for the PZT-5H: $c^*_{11} = c^*_{33} = E_p = 69.8$ GPa, $c_{55} = 23$ GPa, density $\rho_p = 7500$ kg m^{-3}, piezoelectric coupling constants $e^*_{31} = -23.2$ C m^{-2}, $e_{15} = 17$ C m^{-2}, and dielectric constant $\epsilon^*_{33} = 1.73\ 10^{-8}$ F m^{-1}. An initial viscous damping of 0.1% was assumed. The control gain vector $\mathbf{K}_g$ is evaluated using LQR optimal control algorithm. The ponderation matrices $\mathbf{Q}$ and $\mathbf{R}$ are considered to be $\mathbf{Q} = \gamma\mathbf{I}$ and $\mathbf{R} = \mathbf{I}$, giving the same control weight γ for all states. One to three actuators are considered, each of them having same length a and being at position $d_{ck} = 15(3k-1)$ mm ($k = 1,2,3$). By default, three actuators are considered.

The numerical analysis, presented here, consists in evaluation of the active damping, for each parameter variation, supplied by both mechanisms for the first four natural bending modes of the sandwich beam. Therefore, to compare different configurations with different parameters, two basic parameters are fixed: the excitation $\mathbf{F}_m$ and the maximum control voltage $\tilde{\varphi}^{max}$. The free end of the beam is excited by a transverse impulse excitation, which produces a maximum open-loop deflection of $w(L) = 5$ mm. An iterative algorithm, shown in Figure 4, was developed to evaluate the control gain, such that the maximum supplied voltage is $\tilde{\varphi}^{max}_f = 100$ V. Since the same electric field must be imposed to both actuation mechanisms, the maximum voltage for the shear actuators is the double of that of extension ones, i.e., $\tilde{\varphi}^{max}_c = 200$ V. Limited to these voltages, the damping of the two configurations is evaluated.

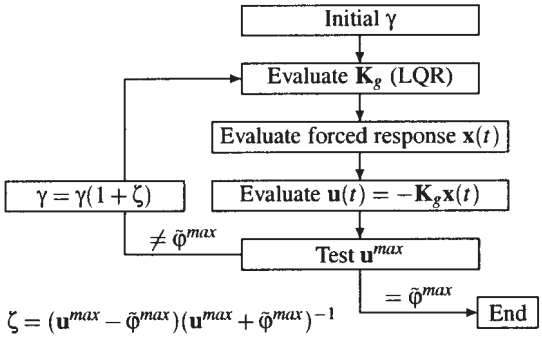

Figure 4. *Algorithm for control gain evaluation* ($2\tilde{\varphi}^{max}_f = \tilde{\varphi}^{max}_c =$ 200 V).

In the first case, the actuator thickness t is varied in the range [0.01, 0.5] mm (note that the shear actuator thickness is $2t$). As it can be seen in Figure 5, the shear actuation mechanism (SAM) provides much larger damping factors for very thin actuators. Moreover, one can see that the effectiveness of the extension actuation mechanism (EAM) is almost independent of the thickness of the actuator, whereas, the shear one is better for a thickness $2t < 0.2$ mm.

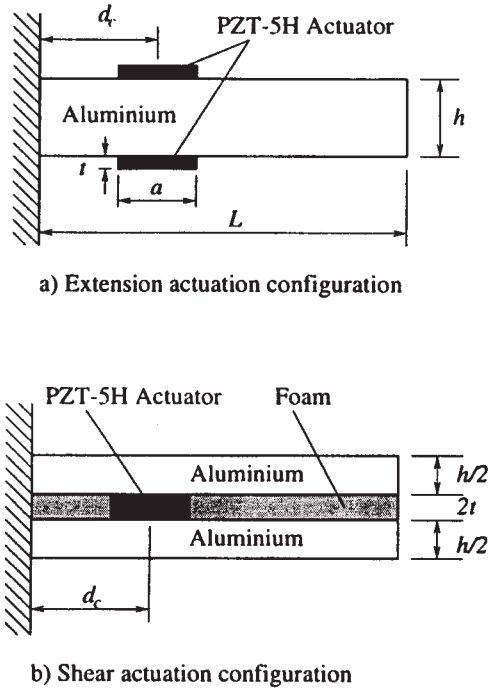

Figure 3. *Cantilever beam, shear and extension actuation configurations.*

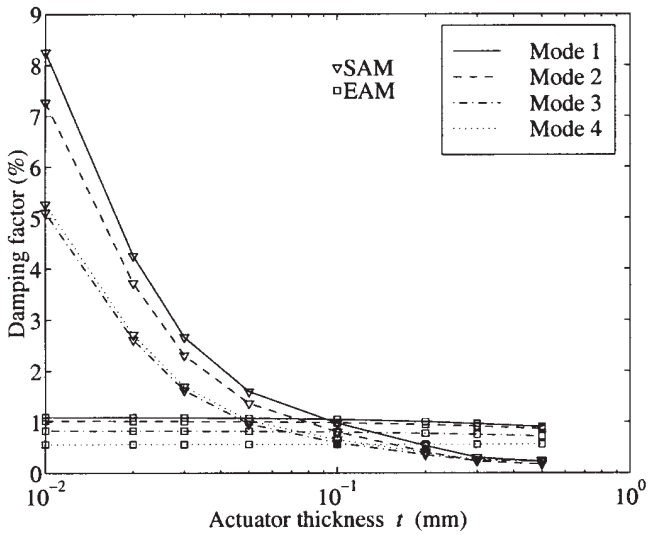

Figure 5. *Variation of first four natural bending modes damping with actuator thickness.*

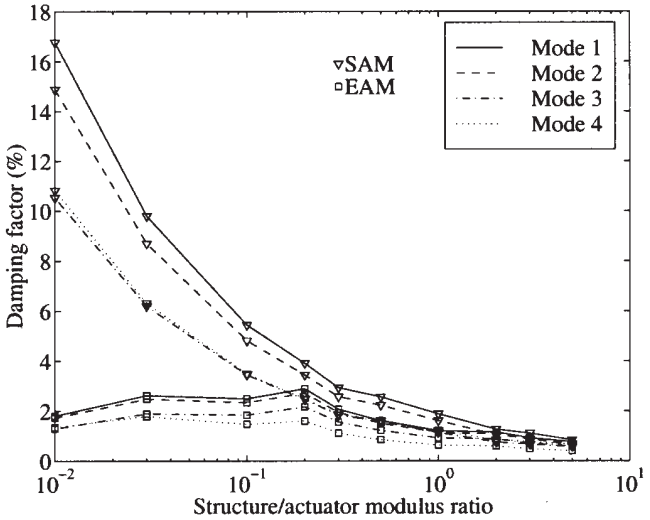

Figure 6. *Variation of first four natural bending modes damping with structure/actuator modulus ratio.*

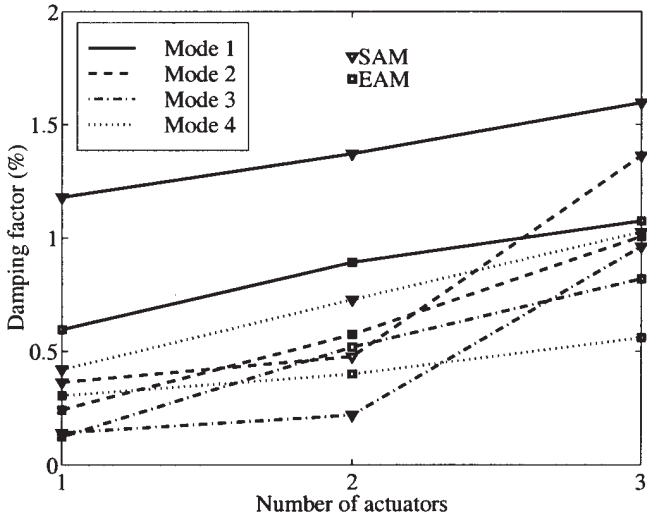

Figure 8. *Variation of the first four natural bending modes damping with number of actuators.*

Next, the effect of the structure stiffness on the active damping is analyzed. To this end, the damping factor is evaluated for several structure/actuator Young's modulus ratios (E_b/E_p). The results, presented in Figure 6, suggest a superiority of the shear actuation mechanism over the extension one for softer structures ($E_b/E_p < 1$). Moreover, shear actuators performance is highly dependent on structure stiffness, whereas, that of extension ones is not, even if the results suggest an optimal medium stiffness ratio ($E_b/E_p = 0.2$). It is important to note that these results are subjected to a variation in the maximum open-loop deflection amplitude since, as the stiffness of the beam decreases, this amplitude increases for a fixed impulse magnitude.

Since the shear actuation mechanism requires the use of an extra-material (here, a foam) to cover the rest of the core layer, it is important to investigate the influence of its material properties. Figure 7 presents the variation of the damping factor with the foam modulus multiplying factor f_c ($E_f = 35.3\ f_c$ MPa, $G_f = 12.7\ f_c$ MPa). It indicates that, generally, the increase of the foam stiffness decreases damping. However, although the output weight γ is the same for all modes, each mode damping presents a different optimal foam stiffness, e.g., the third mode damping is optimal for a relatively rigid foam ($f_c = 3$). This means that soft foams may improve the control of some modes, but not of all of them.

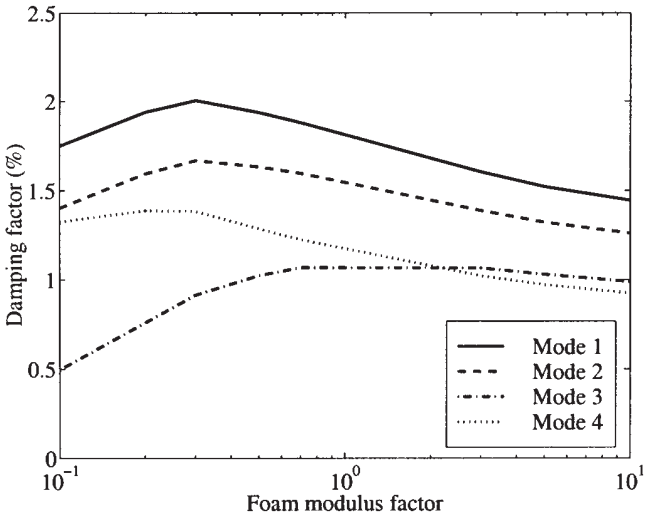

Figure 7. *Variation of first four natural bending modes damping with foam modulus factor* f_c.

The control performance is also dependent on the number of actuators. Generally, several actuators will outperform a single one. Moreover, as the position of actuator defines which modes can be well controlled, several actuators may provide damping over larger frequency range. Figure 8 presents the damping of the first four natural bending modes using one, two and three actuators. It shows that, as expected, the increase in the number of actuators increases the damping factor of all modes. For the extension actuation mechanism, the variation of modal damping with the number of actuators is almost linear. However, for the shear actuation mechanism, although the variation of first and fourth modal damping are also almost linear (approximately +0.2% per actuator), for the second and third modes, the inclusion of a second actuator does not increase much the damping (+0.1%) compared to that of a third one (+0.8%).

CONCLUSIONS

Theoretical and finite element models of an adaptive sandwich beam, capable of dealing with both shear and extension actuation mechanisms, were presented and used to compare active damping performances of such mechanisms for the control of structural bending vibrations of smart beams. It was shown that, for bending actuation, shear actuators induce distributed moments, unlike extension ones which pro-

duce boundary point forces, predicting less problems of debonding and singularities, and better controllability. Using a LQR optimal control law, the influence of important geometrical and material properties on the active damping of the beam was analyzed under maximum applied voltage of $\tilde{\varphi}_c = 2\tilde{\varphi}_f = 200$ V and induced tip transverse deflection of 5 mm. Finite element results show that shear actuators may be better in producing active damping than the generally used extension ones. The shear actuation mechanism was shown to be optimal for a range of thin actuators ($2t < 0.2$ mm) and relatively soft structures. It was observed that the choice of the core filling material is important for the shear actuation mechanism performance, with advantages for softer materials. The increase of the number of actuators enhances the average damping over a broader frequency range. Finally, due to lower stresses in the actuator and better controllability properties, shear actuators are suitable for the vibration control of structures with embedded actuators.

The present study has been extended to the inclusion of embedded shear and/or extension sensors and hybrid piezoelectric-viscoelastic damping treatments (Trindade, Benjeddou and Ohayon, 2000).

NOMENCLATURE

A_i = cross-section area of the layer i
$\mathbf{A}$ = state-space system matrix
a = piezoelectric actuators length
$\mathbf{B}$ = state-space control input matrix
$\mathbf{B}_p$ = state-space perturbation vector
b,L = beam width and length, respectively
$\mathbf{C}$ = state-space output matrix
$\mathbf{C}_v$ = viscous damping matrix
$\hat{\mathbf{C}}$ = control supplied damping matrix
c_{jl},e_{kl},ϵ_{kk} = elastic, piezoelectric and dielectric constants, respectively
δH = virtual variation of electromechanical energy
δT = virtual variation of kinetic energy
δW = virtual variation of external loads work
d_c = piezoelectric actuators center position
E_3,D_3 = transverse electrical field and displacement, respectively
ε_i^b = bending strain of layer i
ε_i^m = axial strain at centerline of layer i (membrane strain)
ε_{c5} = shear strain of layer c
ε_{i1} = axial strain of layer i
$\mathbf{F}_m$ = mechanical loads vector
$\mathbf{F}_e$ = induced electrical loads vector
$\bar{\varphi}_i$ = mean of applied electric potentials on the layer i
$\tilde{\varphi}_i$ = difference of applied electri c potentials on the layer i
φ_i = electric potential in the layer i
φ_i^+,φ_i^- = electric potential at the top and bottom skins of the layer i, respectively
γ = LQR state ponderation factor
h_i = thickness of layer i
I_i = cross-section moment area of the layer i
$\mathbf{K}$ = stiffness matrix
$\mathbf{K}_d$ = derivative control gain matrix
$\mathbf{K}_g$ = control gain matrix
$\mathbf{K}_p$ = proportional control gain matrix
$\hat{\mathbf{K}}$ = control supplied stiffness matrix
$\mathbf{M}$ = mass matrix
N_i,M_i,Q_i = point normal, moment and shear resultants on layer i, respectively
n_i,m_i,q_i = distributed normal, moment and shear resultants on layer i, respectively
$\mathbf{Q}$ = LQR state ponderation matrix
$\mathbf{q}$ = degrees of freedom vector
$\mathbf{R}$ = LQR input ponderation matrix
ρ_i = mass density of the layer i
σ_1,σ_5 = axial and shear stresses, respectively
t = piezoelectric actuators thickness
$\bar{u}$ = mean of the axial displacements of surface layers centerlines
$\bar{u}_1, \tilde{u}_1, w_1, w_1'$ = displacements and rotation of element node 1
$\bar{u}_2, \tilde{u}_2, w_2, w_2'$ = displacements and rotation of element node 2
u_i = axial displacement of the centerline of the layer i
$\tilde{u}$ = difference between the axial displacements of surface layers centerlines
$\hat{u}_i$ = axial displacement of the layer i
w = transverse displacement of beam centerline
$\mathbf{x}$ = state vector
x,z = axial and transverse coordinates
$\mathbf{y}$ = state-space output vector
z_k = distance to centerline of surface layer k (k = a,b)

Subscripts

e,me = state for electrical or mechanical-electrical coupling contributions (piezoelectric)
f = states for quantities related to sandwich surface layers
i = states for beam layers a, b or c
j = states for quantities related to extension (f) and shear (c) actuation mechanisms
k = states for surface layers a or b
m = states for mechanical contributions

Superscripts

$*$ = states for modified material constants
b = states for bending contributions
c = states for core material constants

f = states for surface layers material constants
m = states for membrane contributions
s = states for shear contributions

REFERENCES

Baz, A. 1997. "Boundary control of beams using active constrained layer damping," *J. Vib. Acoust.,* 119:166–172.

Benjeddou, A. 2000. "Advances in finite element modeling of adaptive structural elements: a survey," *Comput. Struct.*, 76(1–3): 347–363.

Benjeddou, A., Trindade, M. A. and Ohayon, R. 1997. "A unified beam finite element model for extension and shear piezoelectric actuation mechanisms," *J. Intell. Mater. Syst. Struct.,* 8(12):1012–1025.

Benjeddou, A., Trindade, M. A. and Ohayon, R. 1999a. "Two models for two actuation mechanisms: A comparison," In Weber, H. I., Gonçalves, P. B., Jasiuk, I., Pamplona, D., Steele, C. R., and Bevilacqua, L, eds., *Applied Mechanics in the Americas,* vol. 8, pp. 1545–1548, Rio de Janeiro (Brazil), January. AAM/ABCM.

Benjeddou, A., Trindade, M. A. and Ohayon, R. 1999b. "New shear actuated smart structure beam finite element," *AIAA J.,* 37(3):378–383.

Benjeddou, A., Trindade, M. A. and Ohayon, R. 2000. "Piezoelectric actuation mechanisms for intelligent sandwich structures," to appear in *Smart Mater. Struct.,* 9.

Bent, A. A., Hagood, N. W. and Rodgers, J. P. 1995. "Anisotropic actuation with piezoelectric fiber composites," *J. Intell. Mater. Syst. Struct.,* 6:338–349.

Chandra, R. and Chopra, I. 1993. "Structural modeling of composite beams with induced-strain actuators," *AIAA J.,* 31:1692–1701.

Crawley, E. F. and Anderson, E. H. 1990. "Detailed models of piezoceramic actuation beams," *J. Intell. Mater. Syst. Struct.,* 1:4–25.

Hagood, N. W., Kindel, R., Ghandi, K. and Gaudenzi, P. 1993. "Transverse actuation of piezoceramics using interdigitated surface electrodes," *North American Conf. on Smart Struct. & Mater.,* SPIE 1917, 341 –352.

Huang, S.C., Inman, D.J. and Austin, E.M. 1996. "Some design considerations for active and passive constrained layer damping treatments," *Smart Mater. Struct.,* 5:301–313.

Kim, G. et al. 1997. "Composite piezoelectric assemblies for torsional actuators," *Naval Research Lab. and PSU Report NRL/MR/6380-97-7997.*

Rahmoune, M., Benjeddou, A., Ohayon, R. and Osmont, D. 1998. "New thin piezoelectric plate models," *J. Intell. Mater. Syst. Struct.,* 9(12):1017–1029.

Sun, C. T. and Zhang, X. D. 1995. "Use of thickness shear mode in adaptive sandwich structures," *Smart Mater. Struct.,* 4:202–206.

The Institute of Electrical and Electronics Engineers, Inc. 1987. *IEEE Standard on Piezoelectricity n.176–1987.*

Tomlinson, G. R. 1996. "An overview of active/passive damping techniques employing viscoelastic materials," *3rd Int. Conf. on Intell. Mater. & 3rd European Conf. on Smart Struct. & Mater.* SPIE 2779, 656–669.

Trindade, M. A., Benjeddou, A. and Ohayon, R. 2000. "Modeling of frequency-dependent viscoelastic materials for active-passive vibration damping," to appear in *J. Vib. Acoust.*, 122(2).

Varadan, V., Lim, Y. -H. and Varadan, V. 1996. "Closed loop finite-element modeling of active/passive damping in structural vibration control," *Smart Mater. Struct.,* 5:685–694.

Zhang, X. D. and Sun, C. T. 1996. "Formulation of an adaptive sandwich beam," *Smart Mater. Struct.,* 5:814–823.